Compact UWB Slotted Monopole Antenna with Diplexer for Simultaneous Microwave Energy Harvesting and Data Communication Applications

Geriki Polaiah[*], Krishnamoorthy Kandasamy, and Muralidhar Kulkarni

Abstract—This paper proposes a new integration of compact ultra-wideband (UWB) slotted monopole antenna with a diplexer and rectifier for simultaneous energy harvesting and data communication applications. The antenna is composed of four symmetrical circularly slotted patches, a feed line, and a ground plane. A slotline open loop resonator based diplexer is implemented to separate the required signal from the antenna without extra matching circuit. A microwave rectifier based on the voltage doubler topology is designed for RF energy harvesting. The prototypes of the proposed antenna, diplexer, and rectifier are fabricated, measured, and compared with the simulation results. The measurement results show that the fractional impedance bandwidth of proposed UWB antenna reaches 149.7% (2.1 GHz–14.6 GHz); the diplexer minimum insertion losses ($|S_{21}|$, $|S_{31}|$) are 1.37 dB and 1.42 dB at passband frequencies; the output isolation ($|S_{23}|$) is better than 30 dB from 1 GHz to 5 GHz; and the peak RF-DC conversion efficiency of the rectifier is 32.8% at an input power of -5 dBm. The overall performance of the antenna with a diplexer and rectifier is also studied, and it is found that the proposed new configuration is suitable for simultaneous microwave energy harvesting and data communication applications.

1. INTRODUCTION

Simultaneous wireless power transmission and communication is a promising technology that is intended to transmit power in free-space without wires and also provides data communication. In the era of green communication, wireless sensor networks, and the Internet of Things (IoT), this technology [1] could play a significant role in power supply and data exchange with numerous sensor nodes that strengthen the reduction in complexity of sensor networks. In wireless power transmission (WPT), the rectifying antenna called rectenna plays an important role in the process of receiving and rectifying of high frequency radio waves [2]. In the recent past, aperture coupled feeding rectenna with all polarization receiving capability [3], coplanar waveguide fed antenna [4] with a single-stage Cockcroft Walton rectifier, electrically small Huygens dipole rectenna [5], and dual-band rectenna using tree-like monopole antenna with Greinacher rectifier topology [6] have been reported. In [7], a single band 2×2 patch element rectenna array is developed for input powers greater than 20 dBm, but it is not suitable for low input RF energy harvesting applications. Some single-band rectenna arrays operating at 2.45 GHz are reported in [8–10], but the size of the rectennas is large. Similarly, broadband antennas are reported in [11–19] especially for mobile and WLAN energy harvesting, but these antennas have less impedance bandwidth. The aforementioned prototypes are useful only for the collection of ambient microwave power and convert the received power into electricity (DC). In addition to this, printed

aperture coupled and Huygens antennas with dual ports and two individual feed lines, out of which one for energy harvesting and the other for data communication, are reported in [20–22], but these designs are found to be complex with two substrates, and also these antennas operate only at single and dual-band frequencies. A new antenna to overcome all the above problems is desirable for Simultaneous Wireless Information and Power Transfer (SWIPT) applications with a new configuration. For this, a printed compact microstrip line diplexer is inserted between the antenna and rectifier that is suitable for simultaneous wireless power transmission and communication. The diplexer is a microwave device used to split or combine two different required frequency signals. Recently, the stub loaded resonators [23, 24], microstrip lines based triple-mode resonator with planar elliptical structure [25], split ring resonator, and multi resonator-coupled diplexers [26, 27], stub loaded three line parallel coupled structure [28], direct-feed coupled-resonator diplexer [29], microstrip diplexer using interdigital capacitors [30], half and quarter-wavelength resonators [31], mixed electromagnetic coupling and T-junction stub-loaded diplexers [32–34] have been reported. In addition, multiband antennas using metamaterial transmission lines, low profile metamaterial band-pass filter, and metamaterial-inspired quad-band notch filter are reported in [35–38]. In [23, 26–30], out of three ports of the diplexer, two ports are adjacent to each other. So, the integration of other devices like antenna and rectifier to these two ports in the diplexer structures is not flexible. Even though there is a sufficient gap among the three ports in [33], the size of the diplexer is large. To design a compact diplexer with integration flexibility, the diplexer structure that consists of slotted open-loop resonators coupled with microstrip feed lines is preferable.

In this article, we propose a simple planar compact ultra-wideband (UWB) slotted monopole antenna with a diplexer and voltage doubler rectifier for simultaneous microwave wireless power transmission and data communication. The proposed new configuration reveals that the antenna transfers the received radiofrequency power to the input port of the diplexer for the separation of two different frequencies through two different ports, one for communication and the other for wireless power transmission. Unlike [20–22], the proposed antenna possesses a single port, single substrate, and wide bandwidth of 12.5 GHz. Unlike [26–30], the proposed compact diplexer has an advantage of simple design, easy fabrication, and flexible integration to other devices. Design details and result analysis of the proposed antenna are mentioned in Section 2. The diplexer design configuration and results are described in Section 3. Similarly, the schematic diagram and fabrication prototype of the proposed rectifier with the comparison of simulation and measured results are mentioned in Section 4. A detailed comparison of the proposed antenna, diplexer, and rectifier with previously reported designs in literature is also tabulated. Finally, the conclusion of this paper is described in Section 5.

2. UWB MONOPOLE ANTENNA

2.1. Antenna Design Details

Figure 1 shows the geometry and dimensions of three different configurations of the proposed compact UWB slotted monopole antenna. The antenna in configuration-1 consists of four symmetrical circular patches with a similar radius of 7 mm joint together to form a symmetrical quatrefoil structure on the front side of the antenna and the truncated ground plane on the backside of the antenna with a height of 11.9 mm. The simulations are carried out by changing the radius and position of circular patches and height of the ground plane to obtain the wideband of antenna that achieves the bandwidth of at least 2 GHz. After that, another four symmetrical circular slots with a similar radius of 3.6 mm etched on the circular patches to improve the bandwidth of the antenna are shown in configuration-2. The simulations are continued by varying the height of the ground plane, radius, and position of circular slots to further enhance the bandwidth of the antenna. The advantage of this design configuration is that the electrical length of the antenna shrinks whereas the performance of the antenna in terms of bandwidth improves predominantly by 3.5 GHz. In the next proposed design of configuration-3, the dimension of main radiator of the antenna does not change, but one end of the ground plane is truncated by a small rectangular slot to extend the bandwidth of the antenna to UWB. With this design, the simulation bandwidth of the antenna is improved by 10.8 GHz, and the operating frequency is extended from 2.1 GHz to 12.9 GHz effectively. The proposed antenna is designed on a low-cost FR4 substrate material ($\varepsilon_r = 4.4$ and $\tan\delta = 0.025$) with a compact dimension of $L \times W \times h$ ($43 \times 38 \times 1.6\,\mathrm{mm}^3$). The antenna is connected to a $50\,\Omega$ microstrip feed line with a width of 3.1 mm to receive the maximum radio

frequency power from the source. The required simulations of the proposed antenna are carried out using the full-wave electromagnetic simulator of CST STUDIO SUITE. The proposed antenna provides a good gain throughout the operating bandwidth especially at the desired frequencies which is useful for receiving the low input microwave power from the sources. The impedance mismatch losses are minimized with wideband antennas integrated into single or multiband rectifiers. The antenna with symmetric configuration and four crescent-shaped slots reduces the overall dimension and electrical size. The novel characteristics of the proposed antenna design include a symmetrical radiator structure with a truncated ground plane broadening the bandwidth and stable gain. In addition, the antenna shows an omnidirectional radiation pattern preferable for energy harvesting applications. The proposed antenna in configuration-3 (shown in Fig. 1) shows an impedance bandwidth from 2.1 GHz to 12.9 GHz by properly optimize the length and width of a rectangular slot on the ground plane. The antenna in configuration-2 (shown in Fig. 1) without a slot in the ground plane provides an impedance bandwidth from 2.1 GHz to 5 GHz only.
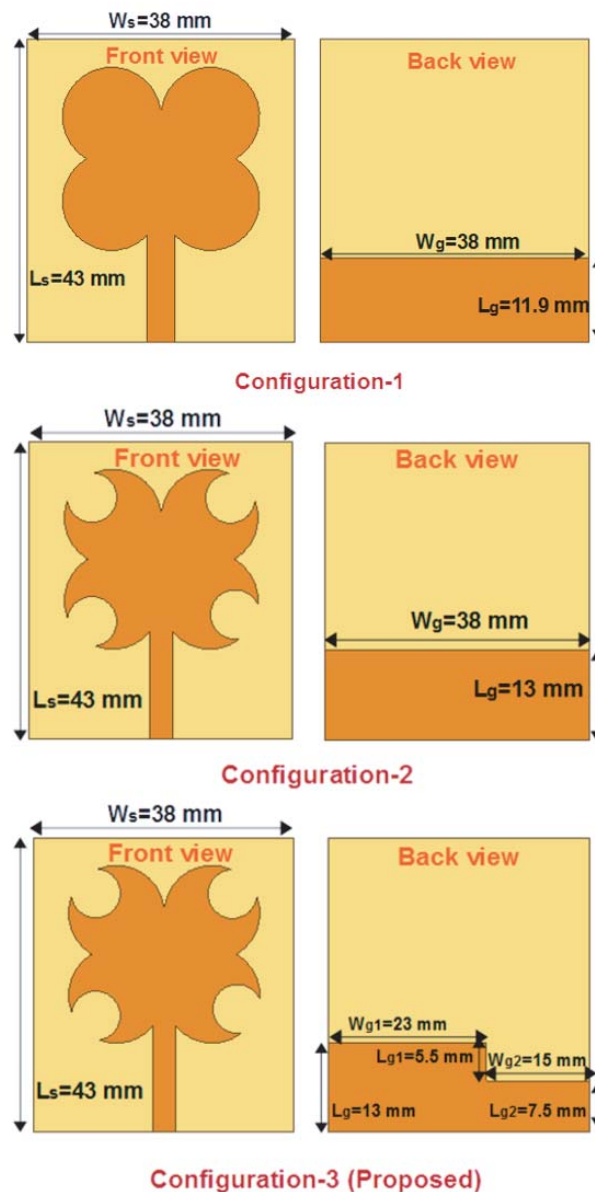
Figure 1. Geometry and dimensions of the monopole antenna in three different configurations.

2.2. Simulation and Measurement Results

The antenna simulation results of reflection coefficient versus frequency in three different configurations are shown in Fig. 2(a). The simulation result of antenna configuration-1 shows the bandwidth of more than 2 GHz with a frequency range from 2.1 GHz to 4.3 GHz and impedance bandwidth of more than 20 dB. The bandwidth is improved by 3.5 GHz with etching circular slots on the circular patches and a frequency range from 2.1 GHz to 5.6 GHz with the design of configuration-2. The proposed antenna (configuration-3) simulation bandwidth of more than 10 GHz (2.1 GHz to 12.9 GHz) is enhanced by the rectangular slot positioned on a suitable place of one end of the ground plane. The proposed antenna bandwidth is more than the bandwidth licensed by the Federal Communications Commission (FCC) from 3.1 GHz to 10.6 GHz. After the completion of all the required simulations, the final design of the proposed antenna shown in configuration-3 is fabricated on an FR4 substrate material using the LPKF ProtoMat S103 PCB fabrication machine available in the laboratory. A 50 Ω internal impedance SMA connector is connected to the antenna feed line using soldering tools. First, the magnitude of reflection coefficient $|S_{11}|$ (dB) is measured using the Agilent Technologies E8363C PNA network analyzer at port-1 and compared with the simulation result. Simulated and measured results of $|S_{11}|$ (dB) versus frequency of the proposed UWB slotted monopole antenna (configuration-3) are shown in Fig. 2(b). The measured result is in good agreement with the simulation one, and the measured -10 dB fractional impedance bandwidth of 149.7% (2.1 GHz–14.6 GHz) is obtained. The gain and radiation patterns of the proposed antenna are measured using an antenna measurement system available in the laboratory which is shown in Fig. 7. In this measurement setup, a standard horn antenna with a gain varying from 3 dB to 16 dB in a frequency range from 0.8 GHz to 18 GHz as a transmitting antenna is positioned in the transmitting section, and it is connected to port-2 of the network analyzer. Similarly, the proposed antenna in receiving mode is mounted on a chamber, and it is connected to port-1 of the network analyzer. The network analyzer is primarily connected to the measurement equipment and computer having pre-installed antenna measurement software. The transmitting and receiving antennas are placed in a far-field distance greater than one meter, and this distance is calculated using a standard far-field equation. Simulated and measured results of gain versus frequency of the proposed UWB slotted monopole antenna in the operating frequency range from 2 GHz to 13 GHz are shown in Fig. 3.

The measured gains of 2.5 dB and 2.4 dB are obtained at the operating frequencies of 2.7 GHz and 3.6 GHz, respectively. The measured peak gain of 4.2 dB is obtained at a higher frequency of 12.9 GHz. For the measurement of radiation patterns, the transmitting and receiving antennas are positioned in the measurement system in a similar plane (E-plane and H-plane) for co-polarization
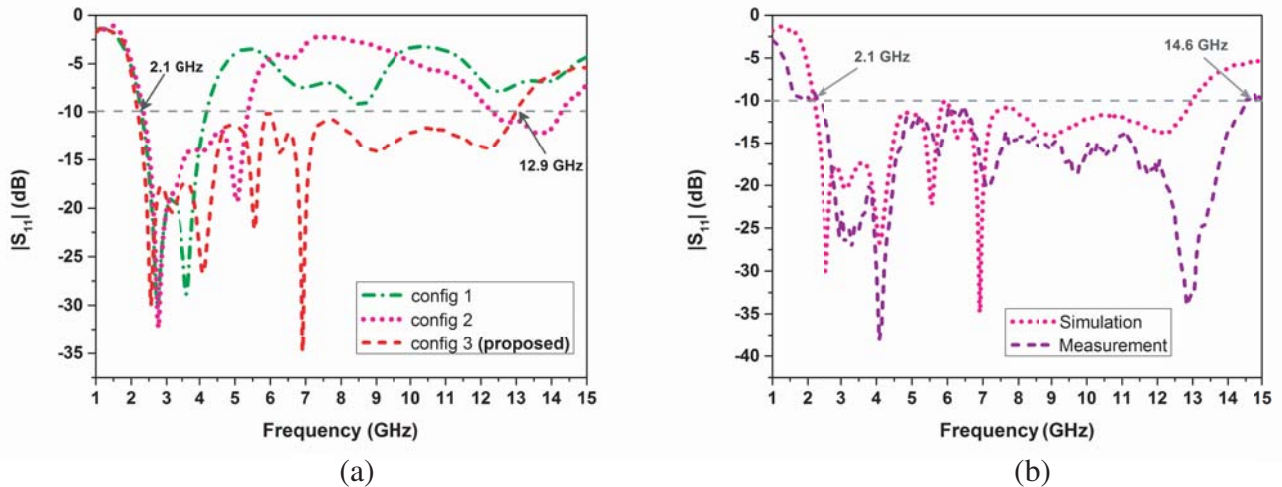
Figure 2. (a) Simulation results of variation of $|S_{11}|$ (dB) versus frequency of the monopole antenna in three different configurations. (b) Simulation and measured results of $|S_{11}|$ (dB) versus frequency of the proposed UWB slotted monopole antenna (Configuration-3).
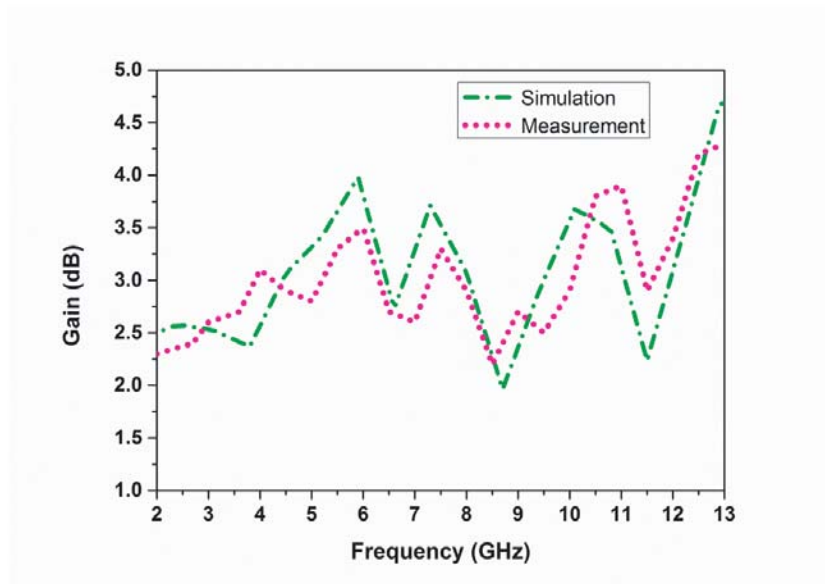
Figure 3. Simulation and measured results of gain (dB) versus frequency of the proposed UWB slotted monopole antenna.
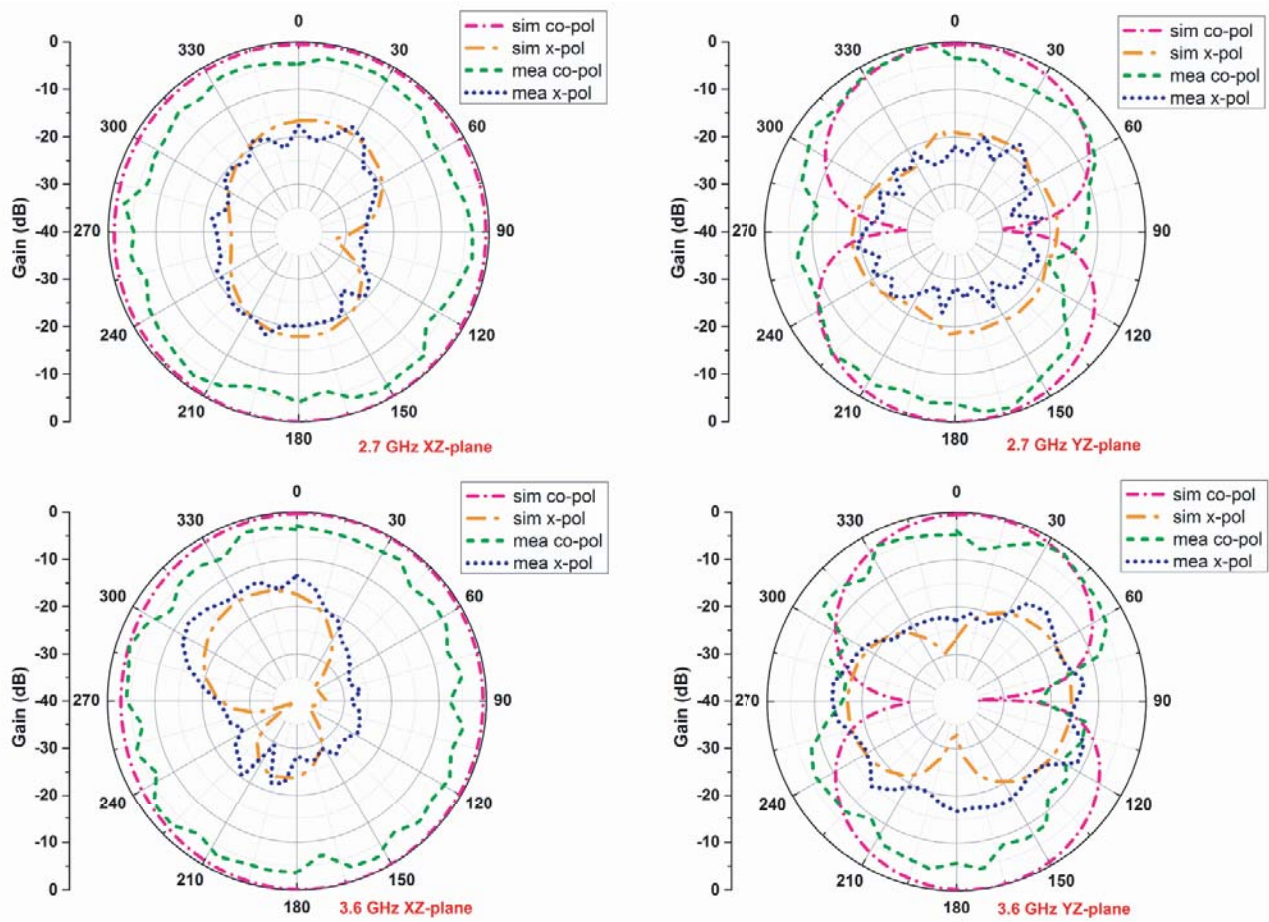
Figure 4. Simulation and measured results of normalized radiation patterns of the proposed UWB slotted monopole antenna at 2.7 GHz and 3.6 GHz frequencies.

and positioned in 90° angle for cross-polarization. The proposed antenna (receiving mode) positioning stand is rotated around 360° with a step angle of 9°. The radiation patterns are measured using the pre-installed antenna measurement software in the computer and recorded. After the measurement of all the required radiation patterns in all the combinations, the measured patterns are normalized to zero the same as the simulation radiation patterns which are normalized using the simulator. Fig. 4 shows the comparison between simulation and measured normalized radiation patterns at the two principal planes of XZ-plane-plane ($\phi = 0°$) and YZ-plane ($\phi = 90°$) at two distinct operating frequencies of 2.7 GHz and 3.6 GHz. It can be observed from the radiation patterns of co-polarization that the proposed antenna presents omnidirectional radiation patterns in XZ-plane and YZ-plane. The simulated and measured cross-polarization levels of less than 20 dB are obtained for the two principal planes at the two operating frequencies of 2.7 GHz and 3.6 GHz. Simulation results of three-dimensional radiation patterns of the proposed UWB slotted monopole antenna at 2.7 GHz and 3.6 GHz frequencies are shown in Fig. 5. It is also observed from the three-dimensional radiation patterns that the proposed antenna exhibits omnidirectional radiation along with the simulation realized gains of more than 2 dB at the above mentioned required frequencies. Similarly, the simulation results of surface current distribution of proposed UWB slotted monopole antenna at the aforementioned frequencies are shown in Fig. 6. The surface current distributions at 2.7 GHz and 3.6 GHz frequencies are simulated at an instant phase of 90°. It can be seen from the results that the current vector is directed with high intensity on the left side of the
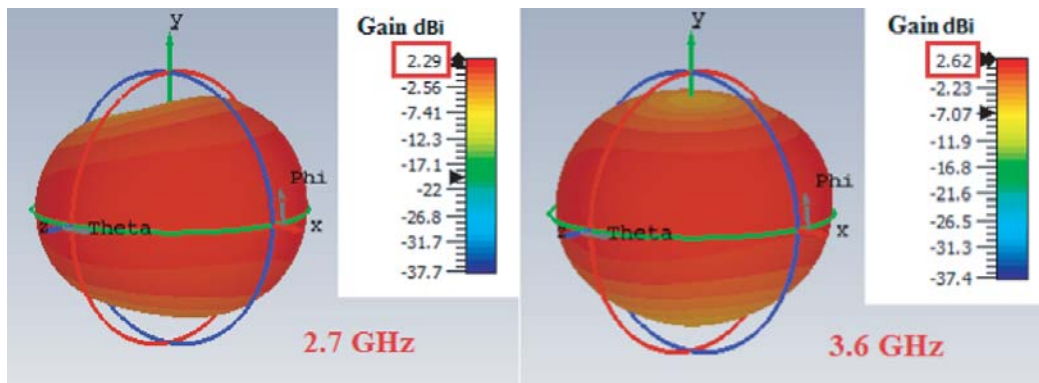
Figure 5. Simulation results of three-dimensional radiation patterns of the proposed UWB slotted monopole antenna at 2.7 GHz and 3.6 GHz frequencies.
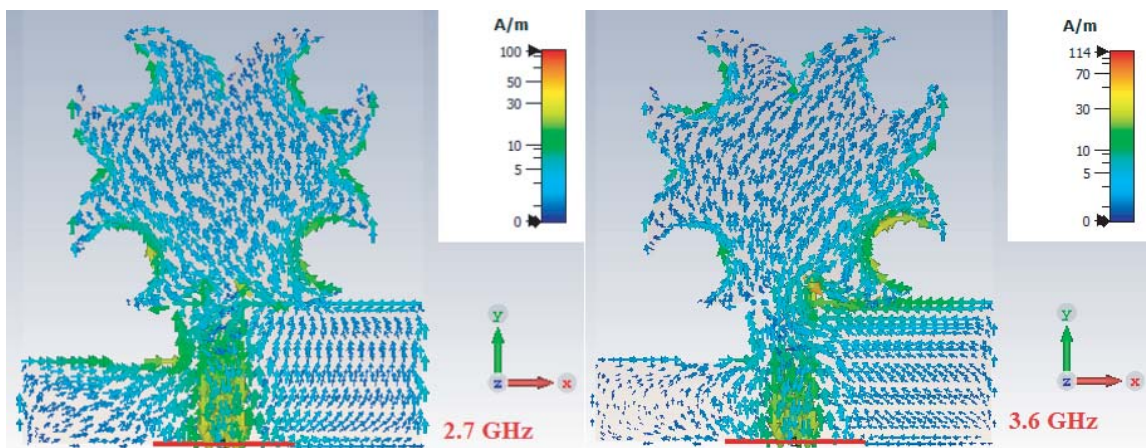
Figure 6. Surface current distribution of the proposed UWB slotted monopole antenna at 2.7 GHz and 3.6 GHz frequencies.
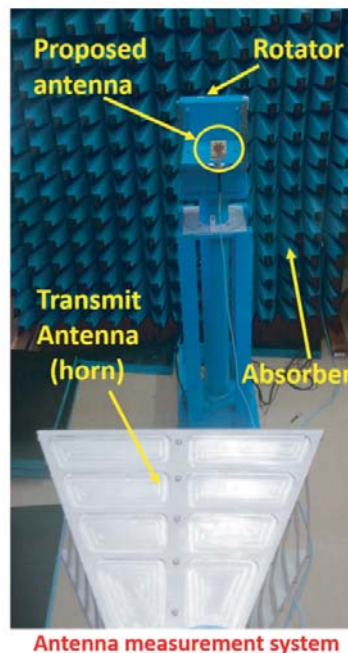
Figure 7. Proposed UWB antenna mounted in a chamber in receiving mode for the measurement of gain and radiation patterns.

truncated ground plane at 2.7 GHz frequency and edges of the circular slots, and with less intensity on the right side of the truncated ground plane at 3.6 GHz frequency. Similarly, the surface current vector is directed with high intensity on the right side of the truncated ground plane at 3.6 GHz frequency, and with less intensity on the left side of the truncated ground plane and edges of the circular slots at 2.7 GHz frequency. The comparison of proposed UWB slotted monopole antenna with recently reported broadband antennas is listed in Table 1, where 'λ' is the free space wavelength at the center frequency of corresponding broadband antenna. The proposed antenna possesses advantages over previously reported antennas in terms of compact size ($43 \times 38\,\text{mm}^2$), enhanced bandwidth of 12.5 GHz, and the measured peak gain of 4.2 dB within the operating band. It is observed from Table 1 that [11, 12, 14] show high gains of greater than 8 dB, but the antennas' sizes are large with less operating bandwidths. The proposed antenna shows more bandwidth, compact size, and more gain than [13, 15, 16].

Table 1. Comparison of the proposed UWB antenna with recently reported broadband antennas.

Reference	Antenna type	Size (mm^2)	Size (λ^2)	Frequency (GHz)	Peak Gain (dB)
[11]	Quasi-Yagi array	190×100	1.26×0.67	1.8–2.2	10.5
[12]	Dual V-shaped slot	135×93	1.06×0.73	2.0–2.7	10.3
[13]	Planar dual-polarized	70×70	0.51×0.51	1.8–2.5	4.1
[14]	Center-fed microstrip patch	90×90	0.57×0.57	1.1–2.7	8.6
[15]	Slotted monopole	50×35	0.42×0.29	2.0–3.1	4.0
[16]	Vivaldi antenna	55×40	0.47×0.34	2.3–2.85	3.0
Proposed	UWB slotted antenna	43×38	1.19×1.05	2.1–14.6	4.2

3. SLOT-LINE OPEN-LOOP RESONATORS BASED DIPLEXER

3.1. Diplexer Design

A microwave diplexer is a passive device that allows the separation of two distinct frequency signals received from the connected antenna and combines the signals for transmission using the same connected antenna [39]. In this work, the proposed antenna is connected to a diplexer that could be considered as a receiving antenna. The diplexer structures recently reported in the literature and mentioned in the introduction are mostly complex and extra matching circuits which are required to match the diplexer input and output ports. The proposed slotline open-loop resonators based diplexer is designed based on the concept of electromagnetic coupling between the resonators [40]. Generally, three types of couplings exist between the resonators namely electric coupling (capacitive coupled), magnetic coupling (inductive coupled), and electromagnetic coupling. In the electric coupling, the maximum electric field density is oriented at the side of an open gap of resonator whereas in the magnetic coupling the maximum magnetic field density is distributed at the opposite side of an open gap of the resonator. The electric fringing field is stronger beside the maximum electric field distribution while the magnetic fringing field is robust near the maximum magnetic field distribution in the resonators. Fig. 8 illustrates the configuration and dimensions of the proposed slotline open-loop resonators based diplexer with a dimension of $L \times W \times h$ ($62 \times 36 \times 1.52\,\text{mm}^3$). The proposed diplexer is composed of two symmetrical open-loop resonator slots, two microstrip feed lines, and one microstrip T-junction. The proposed diplexer is designed on a Rogers 4003C substrate material ($t = 1.52\,\text{mm}$, $\varepsilon_r = 3.3$, $\tan\delta = 0.0027$) for the desired frequencies of 2.7 GHz and 3.6 GHz. The open-loop slots are etched on the top of the ground plane, and microstrip feed lines of $50\,\Omega$ impedance are designed on the bottom of the substrate material. These feed lines are connected to input and output ports for transmitting and receiving microwave power. The dimensional parameters of resonator slots and microstrip feed lines are listed in Table 2.
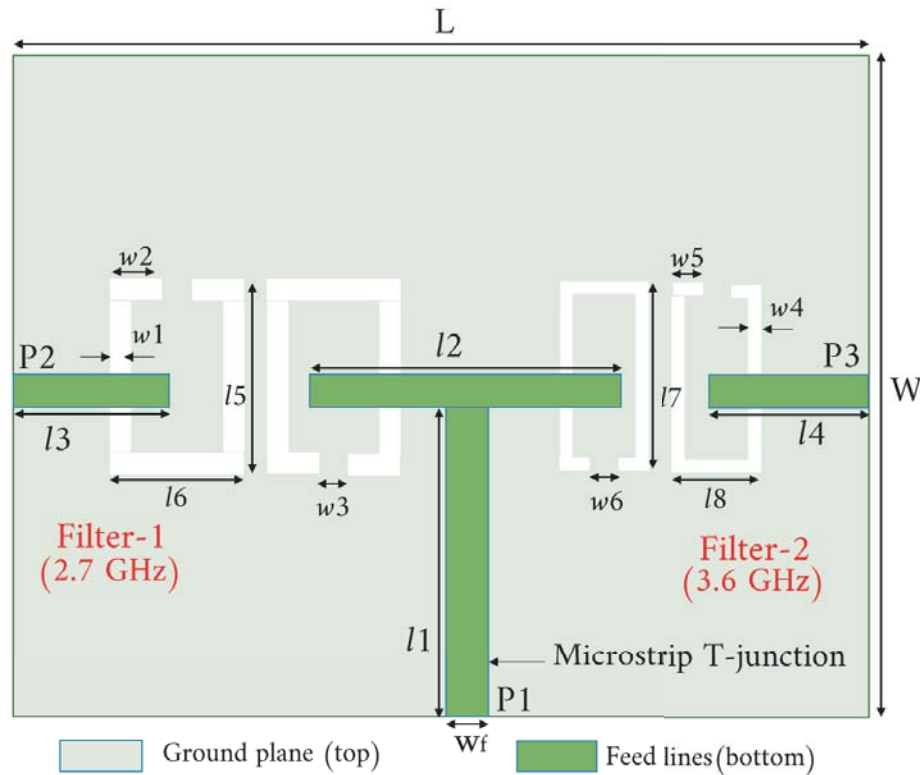
Figure 8. Geometry and configuration of the proposed slot-line open-loop resonators based diplexer.

Table 2. Dimensional parameters of the open-loop slots, microstrip feed lines for the design of proposed diplexer (Unit: mm).

Parameter	Value (mm)	Parameter	Value (mm)
L	62	$l7$	10
W	36	$l8$	6
w_f	3.1	$w1$	1.5
$l1$	18	$w2$	3.8
$l2$	20.5	$w3$	2
$l3$	13	$w4$	1
$l4$	14.2	$w5$	2
$l5$	10.5	$w6$	2
$l6$	9.5		

3.2. Results and Discussion

The required electromagnetic simulations of diplexer structure are performed using a full-wave electromagnetic simulator of CST STUDIO SUITE. After the completion of all the simulations, the diplexer structure is fabricated on the same substrate material mentioned above in the design subsection and fabricated using a similar PCB machine used for the antenna fabrication. The $50\,\Omega$ SMA connectors are soldered on respective places on feed lines for the integration of RF source cables. First, port-1 (P1) of the diplexer is connected to the respective port in PNA network analyzer (E8363C) for the measurement of magnitude of input reflection coefficient ($|S_{11}|$). The measured $|S_{11}|$ result along with the simulation result is plotted in Fig. 9. The measurement and simulation results are in good agreement with each other with a small mismatching of frequency and impedance matching observed due to the variation of input impedances at diplexer ports. The S-parameter of $|S_{11}|$ reaches more than 15 dB for both simulation and measurement. After this, port-1 (P1) and port-2 (P2) of diplexer are connected to similar ports in a network analyzer for the measurement of $|S_{21}|$, and port-1 (P1) and port-3 (P3) are connected to equivalent ports for the measurement of $|S_{31}|$. Simulated and measured results of $|S_{21}|$ and $|S_{31}|$ of the proposed diplexer are shown in Fig. 10(a). The measured results are well matched with simulated ones with the insertion losses of ($|S_{21}|$, $|S_{31}|$) 1.37 dB and 1.42 dB at passband frequencies of
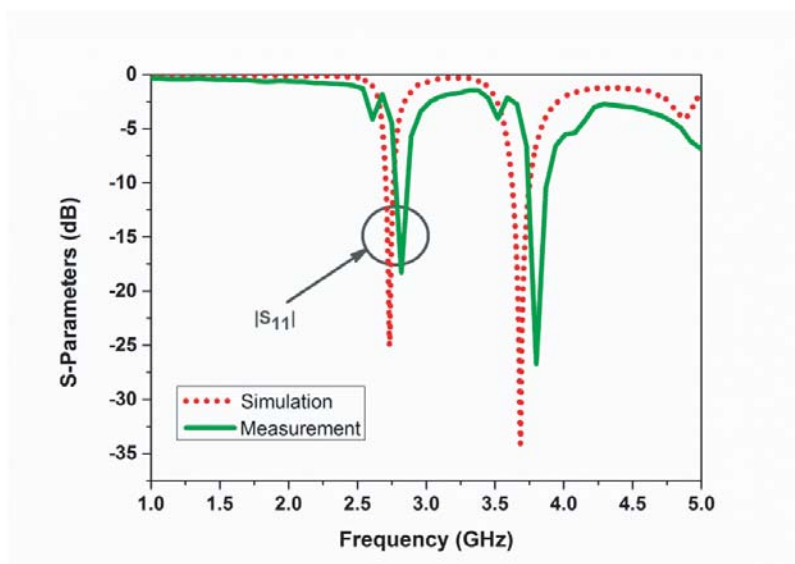
Figure 9. Simulation and measured results of $|S_{11}|$ (dB) versus frequency of the diplexer.

2.7 GHz and 3.6 GHz, respectively. Similarly, the output reflection coefficients of $|S_{22}|$ and $|S_{33}|$ are also measured and compared with the simulation results. Simulated and measured results of $|S_{22}|$ and $|S_{33}|$ at the diplexer output ports (port-2 (P2) and port-3 (P3)) are shown in Fig. 10(b). The two output ports of diplexer are connected to a network analyzer for the measurement of isolation. Simulated and measured results of $|S_{23}|$ between the two output ports of the diplexer are shown in Fig. 10(b). The measured output isolation of greater than 34 dB is obtained for the frequency range from 1 GHz to 5 GHz. In addition, the coupling coefficient ($K = 0.28$) of resonators could also be calculated using the equation mentioned in [40], using lower and upper passband frequencies of 2.7 GHz and 3.6 GHz.
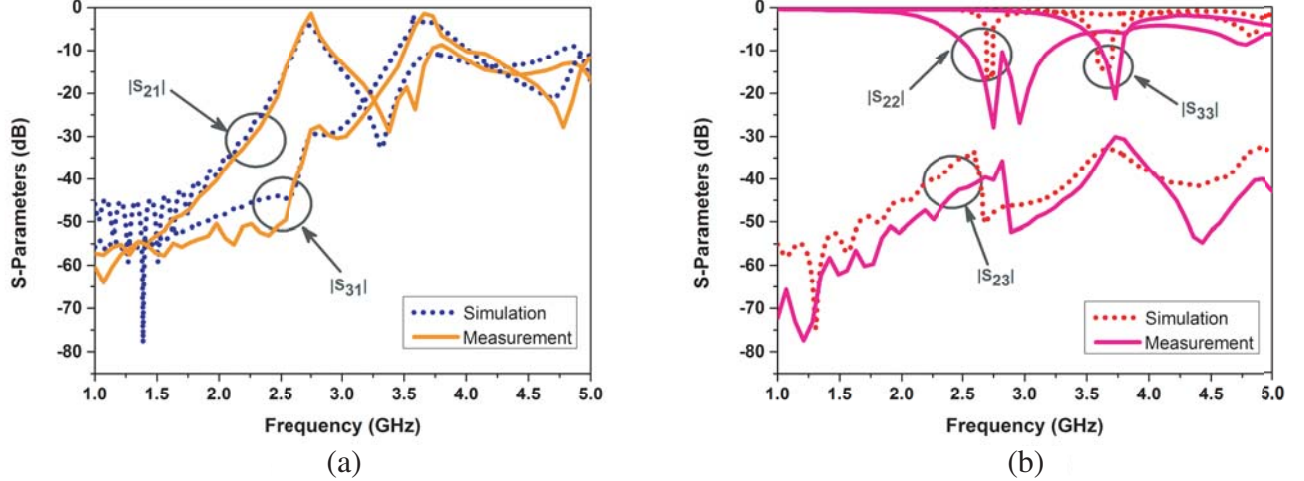
Figure 10. (a) Simulation and measured results of $|S_{21}|$ and $|S_{31}|$ of the diplexer. (b) Simulation and measured results of $|S_{22}|$, $|S_{33}|$, and $|S_{23}|$ of the diplexer.

4. RECTIFIER DESIGN AND RESULT ANALYSIS

4.1. Rectifier Design Details

The transmission line based compact single-stage voltage doubler rectifier circuit is designed at 3.68 GHz (similar to diplexer frequency) operating frequency for the rectification of received radio frequency power into DC. The schematic diagram of the proposed rectifier with a matching network is shown in Fig. 11. The proposed rectifier circuit is composed of an impedance matching network with unequal length open stubs, a voltage doubler, and a load resistor (R_L). The voltage doubler consists of two capacitors C_1 and C_2 of each value 100 pF and two Schottky diodes (D_1 and D_2) from Skyworks. The Schottky diode (SMS7630-079LF) is chosen with a series resistance (R_s) of 20 Ω, breakdown voltage (V_{br}) 2 V, threshold voltage (V_{th}) 147 mV, and zero-bias junction capacitance (C_{j0}) 0.14 pF [41]. Here, the capacitors from Murata act as low pass and DC pass filters in the voltage doubler circuit. The capacitor C_1 stops the harmonic signals generated by the diode to reach the RF source. Similarly, the capacitor C_2 is parallel connected to the load resistor which allows only DC power to the load. The radio frequency signals are similar to sinusoidal signals having an equal amplitude and frequency of continuous positive and negative peaks. The positive peak signal arrives at the input of rectifier. The diode D_2 is ON, and diode D_1 is OFF, then the energy is stored in capacitor C_2. However, the negative peak signal arrives at the input of rectifier. The diode D_1 is ON, and diode D_2 is OFF, then the energy is stored in capacitor C_1. The capacitor C_1 transfers the energy to the capacitor C_2. The proposed rectifier is designed and fabricated on a Rogers 4003C substrate with the characteristics of $\varepsilon_r = 3.3$, $t = 1.52$ mm, and $\tan\delta = 0.0027$, which is sandwiched between the two copper layers of 35 μm thickness. The geometrical dimension of the proposed rectifier is $L \times W \times h$ ($56 \times 37 \times 1.52$ mm^3). The dimensional parameters of microstrip transmission lines used for the design of the rectifier circuit are listed in Table 3. The layout design of the proposed rectifier is also shown in Fig. 12.
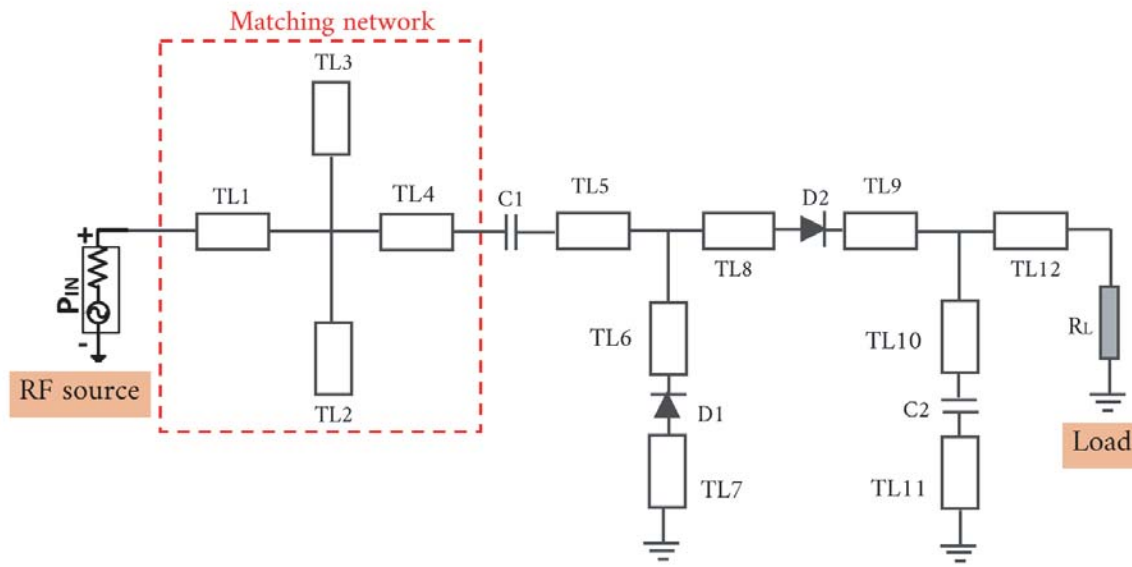
Figure 11. Schematic diagram of the proposed rectifier with a matching network.
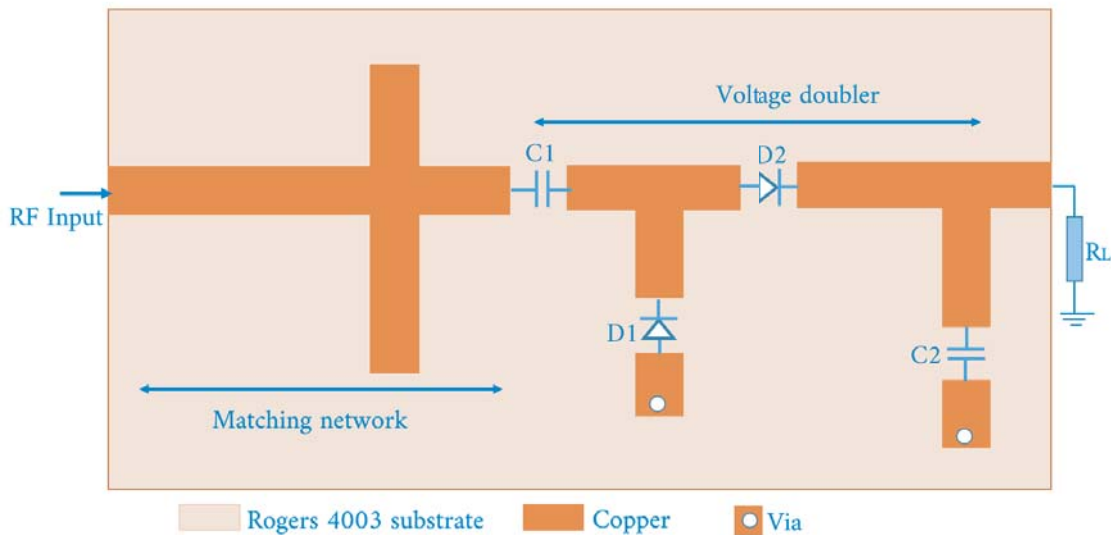
Figure 12. Layout design of the proposed rectifier.

4.2. Simulation and Measurement Results

Design and simulations of the proposed rectifier are performed using Keysight Technologies' high-frequency Advanced Design System simulator. After the completion of required simulations, the rectifier is fabricated on the specified substrate material, and then the essential passive components are soldered on the respective places of printed layout of the rectifier design. The proposed rectifier is measured initially for reflection coefficient magnitude ($|S_{11}|$) by connecting the network analyzer cable directly to the rectifier. Simulated and measured results of $|S_{11}|$ (dB) versus frequency of the proposed rectifier are shown in Fig. 13. The measured result is slightly mismatched with the simulated one because of soldering issues and impedance mismatch losses. Fig. 14(a) shows the simulation results of output

Table 3. Dimensional parameters of microstrip lines used for the design of rectifier circuit (Unit: mm).

Parameter	Width/Length (mm)	Parameter	Width/Length (mm)
TL1	3.1/13.2	TL7	3.1/5.3
TL2	3.1/10.3	TL8	3.1/3.9
TL3	3.1/5.3	TL9	3.1/4.3
TL4	3.1/4.7	TL10	3.1/4.6
TL5	3.1/17.2	TL11	3.1/4.8
TL6	3.1/13.7	TL12	3.1/4.2
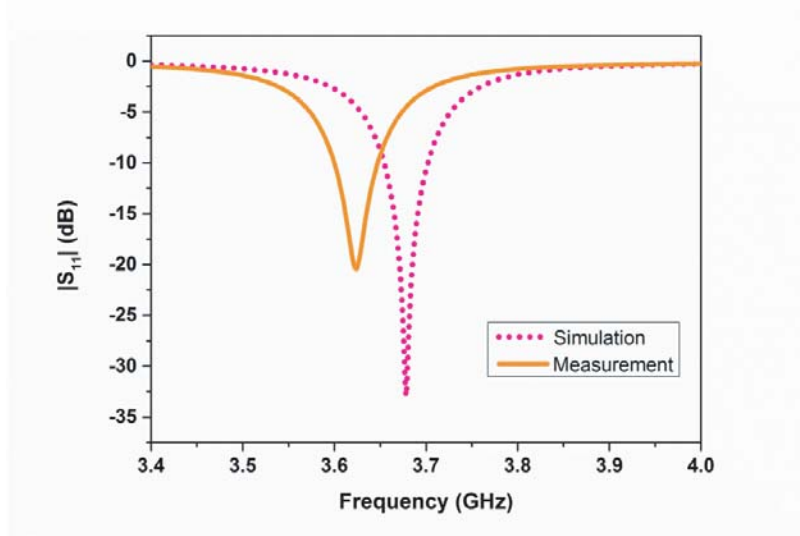
Figure 13. Simulation and measured results of $|S_{11}|$ (dB) versus frequency of the proposed rectifier.
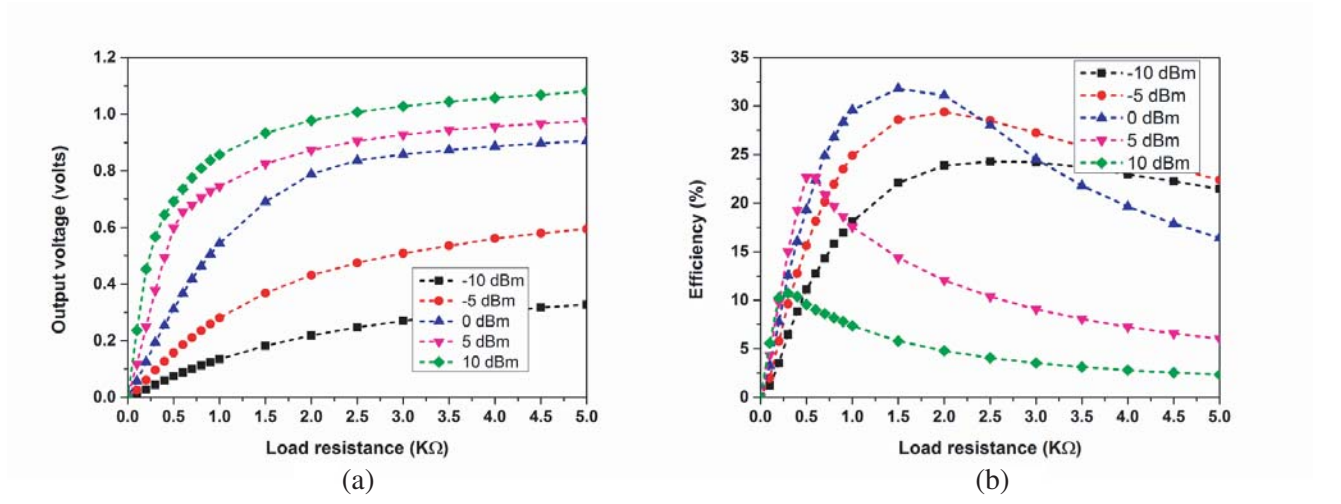
Figure 14. Simulation results of the rectifier for different input powers at 3.68 GHz. (a) Output voltage versus load resistance. (b) Efficiency versus load resistance.

voltage versus load resistance (R_L) of the rectifier for different input powers at 3.68 GHz frequency. In this simulation, the output voltage is noticed by varying the load resistance from 0.1 kΩ to 5 kΩ at the fixed input powers from −10 dBm to 10 dBm. It can be seen from this plot that the maximum

simulation output voltage of 1.09 V is obtained at the input power of 10 dBm. The output voltage (V_0) is saturated beyond the load resistance of 1 kΩ due to the electrical breakdown of the Schottky diode. The simulated RF to DC conversion efficiency of the rectifier is calculated using the following Equation (1).

$$Efficiency(\%) = \frac{V_0^2/R_L}{P_{\text{in}}} \times 100 \tag{1}$$

Simulation results of calculated efficiency versus load resistance (R_L) of the rectifier for different input powers at 3.68 GHz frequency are shown in Fig. 14(b). It can be observed that the maximum simulated efficiency of 32% is obtained at 1.5 kΩ load resistance and 0 dBm input power. It is interesting to note that the efficiency plots are stable from 0.7 kΩ to 3 kΩ for the input powers of −10 dBm, −5 dBm, and 0 dBm. However, very narrow peaks are observed near the load resistance of 0.5 kΩ for the input powers of 5 dBm and 10 dBm. It means that the rectifier possesses an early breakdown at the input powers greater than 0 dBm. So, it is suitable for low input RF powers. However, the output voltage versus input power (P_{in}) for different load resistances was also performed for further analysis of the rectifier. Simulation results of output voltage versus input power (P_{in}) of the rectifier for different load resistances at 3.68 GHz operating frequency are shown in Fig. 15(a). The maximum simulated output voltage of 1.23 V is obtained at an input power of 15 dBm and the load resistance of 4.5 kΩ. There is a small difference in output voltage observed among the load resistances of 2.5 kΩ, 3.5 kΩ, and 4.5 kΩ. Similarly, the RF to DC conversion efficiency is calculated using Equation (1) for the different load resistance values of fixed input powers. Simulation results of calculated efficiency versus input power (P_{in}) of the rectifier for different load resistances at 3.68 GHz frequency are shown in Fig. 15(b). It can be confirmed that the proposed rectifier possesses simulated peak RF to DC conversion efficiency of 32% at the load resistance of 1.5 kΩ and an input power of 0 dBm. The load resistor value of 1 kΩ which is close to 1.5 kΩ is connected to the rectifier after fabrication. Simulation results of output voltage and efficiency versus frequency of the rectifier at optimized values of 1 kΩ load resistance and 0 dBm input power are shown in Fig. 16(a). The voltage and efficiency of rectifier show maximum values at an optimized values of 1 kΩ load resistance and 0 dBm input power. It should be noted that the input impedance and output voltage of the rectifier predominantly depend on input power, load resistance, and frequency. Simulated and measured output voltages and calculated efficiencies versus input power of the proposed rectifier at optimized values of 1 kΩ load resistance and 3.6 GHz frequency are shown in Fig. 16(b). The rectifier SMA port directly connects to network analyzer cable for receiving RF power, and the output voltage is measured using a digital voltmeter. A photograph of output voltage measurement of the proposed rectifier at 15 dBm input power received from the E8363C PNA network analyzer considered as an RF source is shown in Fig. 17. It can be observed that the measured output voltage
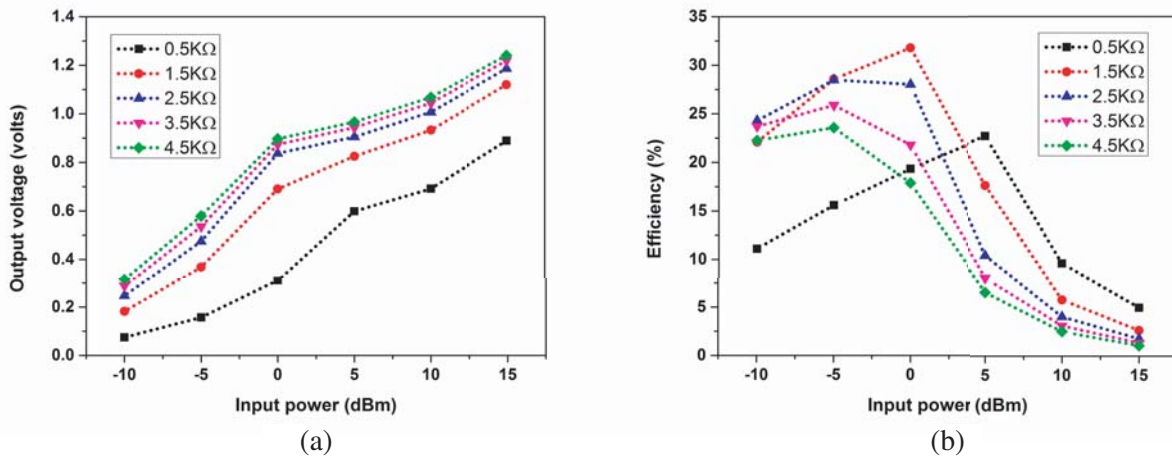
Figure 15. Simulation results of the rectifier for different load resistances at 3.68 GHz. (a) Output voltage versus input power. (b) Efficiency versus input power.
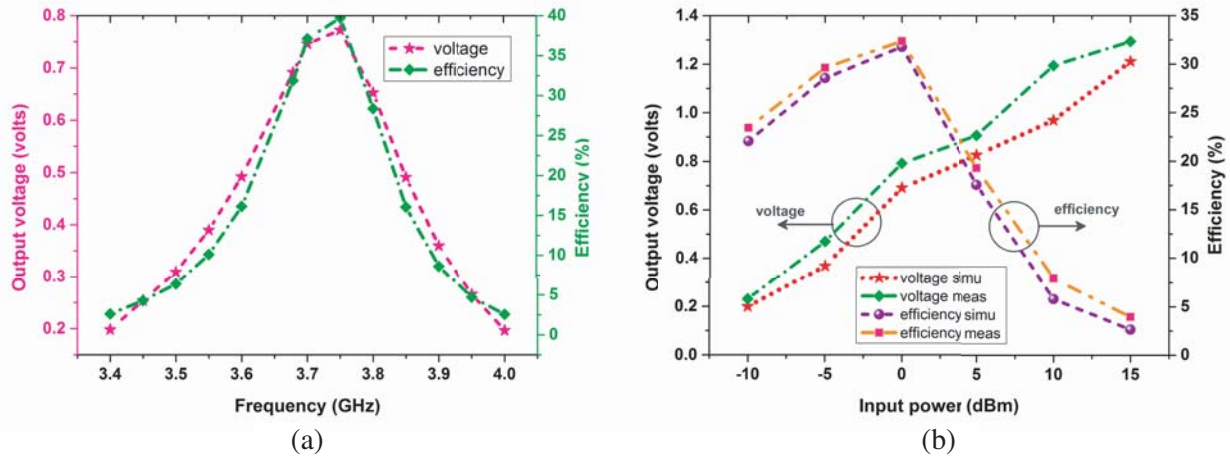
Figure 16. (a) Simulation results of output voltage and efficiency versus frequency of the rectifier at an optimized values of 1 kΩ load resistance and 0 dBm input power. (b) Simulation and measured output voltage and efficiency versus input power at an optimized values of 1 kΩ load resistance and 3.6 GHz frequency.

Figure 17. Photograph of output voltage measurement of the proposed rectifier at 15 dBm input power received from E8363C PNA network analyzer considered as an RF source. (voltage = 1.194 V).

shown in the voltmeter is 1.194 V. The rectifier maximum RF to DC conversion efficiency of 32.8% is obtained at optimized values of 1 kΩ load resistance and 0 dBm input power. After the measurements, the proposed antenna is connected with a diplexer and rectifier using a pair of 50 Ω coaxial connectors for simultaneous microwave energy harvesting and data communication applications. A photograph of the new integration of antenna, diplexer, and rectifier for simultaneous wireless power transmission
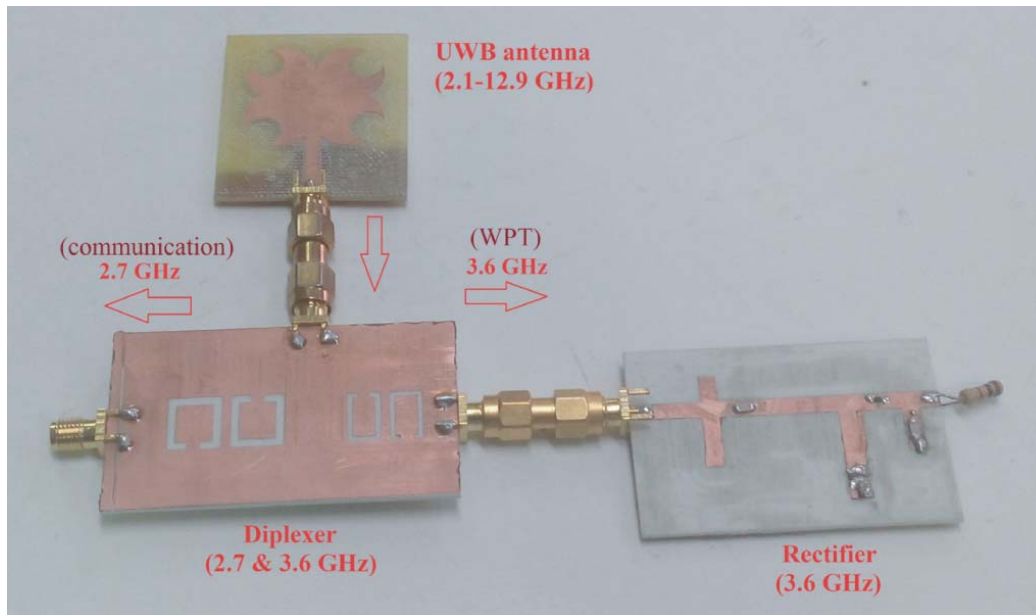
Figure 18. Photograph of the new integration of antenna, diplexer, and rectifier for simultaneous wireless power transmission and data communication.

Table 4. Performance comparison of the proposed diplexer with previous designs in the literature.

Reference	Frequency (GHz)	Size (mm^2)	Size (λ^2)	Insertion loss (dB)	Isolation (dB)
[26]	1.8/2.45	44×17	0.26×0.11	2.8/2.3	> 38
[28]	1.78/2.37	50×43	0.29×0.25	1.54/1.47	> 40
[31]	1.82/2.41	22×40	0.13×0.24	2.2/2.1	> 30
[34]	1.95/2.14	63×58	0.41×0.38	1.2/1.5	> 30
Proposed	2.7/3.6	62×36	0.56×0.32	1.37/1.42	> 34

Table 5. Comparison of the proposed rectifier with previous reported designs in the literature.

Reference	Frequency (GHz)	Load resistance (kΩ)	Input power (dBm)	RF-DC efficiency (%)
[11]	1.84	5	-5	43
[13]	2.45	14.7	-5	47
[14]	2.45	2	-5	28
[15]	2.4	4	-5	42
Proposed	3.6	1	-5	32.8

and data communication is shown in Fig. 18. It should be noted that the antenna in this configuration is considered as transmitting/receiving antenna for the frequency of 2.7 GHz and receiving antenna for the frequency of 3.6 GHz. The comparison tables of diplexer and rectifier with their previous designs in literature are listed in Table 4 and Table 5. In Table 4, 'λ' is the free space wavelength at a lower

frequency of the corresponding diplexer. The insertion loss of the proposed diplexer in Table 4 is lower than that of [26, 28, 31] at resonance frequencies. However, the proposed diplexer output isolation is higher than [31, 34]. In Table 5, the proposed rectifier shows higher RF to DC conversion efficiency than [14] at an input power of -5 dBm and a load resistance of 1 kΩ.

5. CONCLUSION

A novel integration of antenna, diplexer, and rectifier for simultaneous microwave wireless power transmission and data communication application is proposed. The designed prototypes are fabricated, measured, and compared with the simulation results. The proposed antenna possesses the advantages of being planar, compact, ultra-wideband (2.1 GHz to 14.6 GHz), small electrical length, easy to fabricate, and flexible connectivity to other devices. The compact planar diplexer based on the electromagnetic coupling of slotted open-loop resonators is designed and implemented. The rectifier is developed using a voltage doubler for microwave wireless power transmission. The rectifier measured RF-DC conversion efficiency of more than 30% is obtained. The proposed new configuration is well suitable for the emerging application of simultaneous wireless power transmission (energy harvesting) and data communication.

REFERENCES

1. Krikidis, I., T. Stelios, S. Nikolaou, G. Zheng, D. W. Kwan, and R. Schober, "Simultaneous wireless information and power transfer in modern communication systems," *IEEE Communications Magazine*, Vol. 52, 104–110, 2014.
2. Shinohara, N., *Wireless Power Transfer via Radio Waves*, Wiley, Hoboken, 2014.
3. Sun, H. and W. Geyi, "A new rectenna with all polarization receiving capability for wireless power transmission," *IEEE Antennas and Wireless Propagation Letters*, Vol. 15, 814–817, 2016.
4. Awais, Q., Y. Jin, H. T. Chattha, M. Jamil, H. Qiang, and B. A. Khawaja, "A compact rectenna system with high conversion efficiency for wireless energy harvesting," *IEEE Access*, Vol. 6, 35857–35866, 2018.
5. Lin, W., R. W. Ziolkowski, and J. Huang, "Electrically small low-profile, highly efficient Huygens dipole rectennas for wirelessly powering internet of things devices," *IEEE Transactions on Antennas and Propagation*, Vol. 67, No. 6, 3670–3679, 2019.
6. Wang, M., Y. Fan, L. Yang, Y. Li, J. Feng, and Y. Shi, "Compact dual band rectenna for RF energy harvest based on a tree like antenna," *IET Microwaves Antennas and Propagation*, Vol. 13, No. 9, 1350–1357, 2019.
7. Li, X., L. Yang, and L. Huang, "Novel design of 2.45 GHz rectenna element and array for wireless power transmission," *IEEE Access*, Vol. 7, 28356–28362, 2019.
8. Hu, Y. Y., S. Sun, and H. Xu, "Compact collinear quasi Yagi antenna array for wireless energy harvesting," *IEEE Access*, Vol. 8, 35308–35317, 2020.
9. Sun, H., H. He, and J. Huang, "Polarization insensitive rectenna arrays with different power combining strategies," *IEEE Antennas and Wireless Propagation Letters*, Vol. 19, No. 3, 492–496, 2020.
10. Takabayashi, N., N. Shinohara, T. Mitani, M. Furukawa, and T. Fujiwara, "Rectification improvement with flat topped beams on 2.45 GHz rectenna arrays," *IEEE Transations on Microwave Theory and Techniques*, Vol. 68, No. 3, 1151–1163, 2020.
11. Sun, H., Y. X. Guo, M. He, and Z. Zhong, "A dual band rectenna using broadband Yagi antenna array for ambient RF power harvesting," *IEEE Antennas and Wireless Propagation Letters*, Vol. 12, 918–921, 2013.
12. Nie, M. J., X. X. Yang, G. N. Tan, and B. Han, "A compact 2.45 GHz broadband rectenna using grounded coplanar waveguide," *IEEE Antennas and Wireless Propagation Letters*, Vol. 14, 986–989, 2015.

13. Song, C., Y. Huang, J. Zhou, J. Zhang, S. Yuan, and P. Carter, "A high efficiency broadband rectenna for ambient wireless energy harvesting," *IEEE Transactions on Antennas and Propagation*, Vol. 63, No. 8, 3486–3495, 2015.

14. Song, C., Y. Huang, P. Carter, J. Zhou, S. D. Joseph, and G. Li, "Novel compact and broadband frequency selectable rectennas for a wide input power and load impedance range," *IEEE Transactions on Antennas and Propagation*, Vol. 66, No. 7, 3306–3316, 2018.

15. Shi, Y., Y. Fan, Y. Li, L. Yang, and M. Wang, "An efficient broadband slotted rectenna for wireless power transfer at LTE band," *IEEE Transactions on Antennas and Propagation*, Vol. 67, No. 2, 814–822, 2019.

16. Shi, Y., J. Jing, Y. Fan, L. Yang, J. Pang, and M. Wang, "Efficient RF energy harvest with a novel broadband Vivaldi rectenna," *Microwave and Optical Technology Letters*, Vol. 60, 2420–2425, 2018.

17. Lee, C. H. and Y. H. Chang, "Design of a broadband circularly polarized rectenna for microwave power transmission," *Microwave and Optical Technology Letters*, Vol. 57, 702–706, 2014.

18. Lu, P., K. M. Huang, Y. Yang, F. Cheng, and L. Wu, "Frequency reconfigurable rectenna with an adaptive matching stub for microwave power transmission," *IEEE Antennas and Wireless Propagation Letters*, Vol. 18, No. 5, 956–960, 2019.

19. Lu, P., C. Song, and K. M. Huang, "A compact rectenna design with wide input power range for wireless power transfer," *IEEE Transactions on Power Electronics*, Vol. 35, No. 7, 6705–6710, 2020.

20. Yang, X. X., C. Jiang, A. Z. Elsherbeni, F. Yang, and Y. Q. Wang, "A novel compact printed rectenna for data communication systems," *IEEE Transactions on Antennas and Propagation*, Vol. 61, No. 5, 2532–2539, 2013.

21. Zhu, G. L., J. X. Du, X. X. Yang, Y. G. Zhou, and S. Gao, "Dual-polarized communication rectenna array for simultaneous wireless information and power transmission," *IEEE Access*, Vol. 7, 141978–141986, 2019.

22. Lin, W. and R. W. Ziolkowski, "Electrically small Huygens antenna-based fully integrated wireless power transfer and communication system," *IEEE Access*, Vol. 7, 39762–39769, 2019.

23. Li, X. T., F. Cheng, P. Lu, and K. Huang, "High isolation diplexer using stub-loaded resonators," *Electronic Letters*, Vol. 55, No. 14, 800–801, 2019.

24. Zhang, Z. C., S. W. Wong, J. Y. Lin, H. Liu, L. Zhu, and Y. He, "Design of multistate diplexers on uniform and stepped-impedance stub-loaded resonators," *IEEE Transactions on Microwave Theory and Techniques*, Vol. 67, No. 4, 1452–1460, 2019.

25. Wong, S. W., B. L. Zheng, J. Y. Lin, Z. C. Zhang, Y. Yang, L. Zhu, and Y. He, "Design of three-state diplexer using a planar triple-mode resonator," *IEEE Transactions on Microwave Theory and Techniques*, Vol. 66, No. 9, 4040–4046, 2018.

26. Xiao, J. K., Y. Li, and J. G. Ma, "Compact and high isolated triangular split-ring diplexer," *Electronic Letters*, Vol. 54, No. 10, 661–663, 2018.

27. Xiao, J. K., M. Zhang, and J. G. Ma, "A compact and high-isolated multi resonator-coupled diplexer," *IEEE Microwave and Wireless Components Letters*, Vol. 28, No. 11, 999–1001, 2018.

28. Chen, X., X. Yu, and S. Sun, "Design of high-performance microstrip diplexers with stub-loaded parallel-coupled lines," *Electronic Letters*, Vol. 53, No. 15, 1052–1054, 2017.

29. Deng, P. H., R. C. Liu, W. D. Lin, and W. Lo, "Design of a microstrip low-pass-bandpass diplexer using direct-feed coupled-resonator filter," *IEEE Microwave and Wireless Components Letters*, Vol. 27, No. 3, 254–256, 2017.

30. Bui, D. H. N., T. P. Vuong, B. Allard, J. Verdier, and P. Benech, "Compact low-loss microstrip diplexer for RF energy harvesting," *Electronic Letters*, Vol. 53, No. 8, 552–554, 2017.

31. Yan, J. M., H. Y. Zhou, and L. Z. Cao, "Compact diplexer using microstrip half and quarter wavelength resonators," *Electronic Letters*, Vol. 52, No. 19, 1613–1615, 2016.

32. Xiao, J. K., M. Zhu, Y. Li, L. Tian, and J. G. Ma, "High selective microstrip bandpass filter and diplexer with mixed electromagnetic coupling," *IEEE Microwave and Wireless Components Letters*, Vol. 25, No. 12, 781–783, 2015.

33. Chen, C. F., C. Y. Lin, B. H. T. Seng, and S. F. Chang, "High-isolation and high-rejection microstrip diplexer with independently controllable transmission zeros," *IEEE Microwave and Wireless Components Letters*, Vol. 24, No. 12, 851–853, 2014.

34. Guan, X., F. Yang, H. Liu, and L. Zhu, "Compact and high-isolation diplexer using dual-mode stub-loaded resonators," *IEEE Microwave and Wireless Components Letters*, Vol. 24, No. 6, 385–387, 2014.

35. Keshavarz, S. and N. Nozhat, "Dual-band Wilkinson power divider based on composite right/left-handed transmission lines," *13th International Conference on Electrical Engineering/Electronics, Computer, Telecommunications and Information Technology (ECTI-CON)*, 2016.

36. Keshavarz, R., M. Danaeian, M. Movahhedi, and A. Hakimi, "A compact dual-band branch-line coupler based on the interdigital transmission line," *19th Iranian Conference on Electrical Engineering*, 2011.

37. Keshavarz, R. and N. Shariati, "Low profile metamaterial band-pass filter loaded with 4-turn complementary spiral resonator for WPT Applications," *27th IEEE International Conference on Electronics, Circuits and Systems (ICECS)*, 2020.

38. Keshavarz, R., Y. Miyanaga, M. Yamamoto, T. Hikage, and N. Shariati, "Metamaterial-inspired quad-band notch filter for LTE band receivers and WPT applications," *33rd URSI General Assembly and Scientific Symposium*, 2020.

39. Keshavarz, S., A. Abdipour, A. Mohammadi, and R. Keshavarzt, "Design and implementation of low loss and compact microstrip triplexer using CSRR loaded coupled lines," *International Journal of Electronics and Communications*, Vol. 111, 1–5, 2019.

40. Hong, J. S. and M. J. Lancaster, "Couplings of microstrip square open-loop resonators for cross-coupled planar microwave filters," *IEEE Transactions on Microwave Theory and Techniques*, Vol. 44, No. 12, 2099–2109, 1996.

41. SMS 7630-079LF Schottky diode datasheet, *Skyworks Solutions*, 2018.